

Supporting information

Cu Overlayers on Tetrahedral Pd Nanocrystals with High-Index Facets for CO₂ Electroreduction to Alcohols

Feng-Yang Zhang, Tian Sheng, Na Tian*, Li Liu, Chi Xiao, Bang-An Lu, Bin-Bin Xu, Zhi-You Zhou and Shi-Gang Sun

Email: tnsd@xmu.edu.cn

State Key Laboratory of Physical Chemistry of Solid Surfaces, Collaborative Innovation Center of Chemistry for Energy Materials, College of Chemistry and Chemical Engineering, Xiamen University, Xiamen 361005, China

Experimental details

Preparation of Tetrahedral Pd nanocrystals (THH Pd NCs) and (111)-faceted Pd NCs

The working electrode is a glassy carbon (GC, $\phi=6$ mm, purchased from Takai Carbon Co., Ltd., Tokyo, Japan) electrode. Prior to experiment, the GC electrode was mechanically polished using sequentially alumina powder of size 5, 1, 0.3 μm . Then it was cleaned in an ultrasonic bath. For a better comparison all potentials are given against the reversible hydrogen electrode (RHE) in this paper. Electrochemical measurements were carried out by PAR 263A potentiostat/galvanostat (EG&G). THH Pd NCs were prepared by the programmed square-wave potential (SWP) method on the GC electrode in 0.2 mM PdCl₂ (99.999%, Alfa Aesar) + 0.1 M HClO₄ (G.R. reagent) solution at ambient temperature. Firstly, the GC electrode was subjected to a potential step from 1.50 V to 0.20 V and stayed for 20 ms to produce Pd nuclei; then an electrochemical square-wave potential treatment with the lower potential limit (E_L) of 0.60 V and upper potential limit (E_U) of 1.01 V at 100 Hz was applied for 45 min for the preparation of THH Pd NCs. The (111)-faceted Pd NCs on GC electrode were electrodeposited at 0.20 V for 500 s. All solutions were prepared using super-pure water (18.2 M Ω cm) generated from a Milli-Q system (Nihon Millipore Ltd).

Cu overlayer preparation The Cu overlayers were prepared by underpotential deposition (UPD) from a solution containing 1 mM CuSO₄ (CuSO₄·5H₂O from Sigma-Aldrich, $\geq 98.0\%$) and 0.5 M H₂SO₄ (G.R. reagent).

Electrocatalytic CO₂ reduction CO₂ reduction was performed in 0.1 M NaHCO₃ (pH=6.8), prepared by bubbling CO₂ through a 0.1 M Na₂CO₃ solution ($\geq 99.999\%$, Sigma-Aldrich). The electrochemical CO₂ reduction experiments were performed in a home-made three-electrode cell at room temperature using a Pt foil as counter electrode and an Hg/Hg₂Cl₂ as reference electrode. The working and counter electrode compartments are separated by a Nafion-115 proton exchange membrane to prevent the oxidation of the CO₂ electroreduction products. The electrocatalytic process was performed by applying a constant potential (-0.36, -0.46 or -0.56 V). The iR drop was compensated during electrolysis. The cathodic compartment was continuously purged with a constant CO₂ (99.999%, Linde) flow rate to ensure the saturation of CO₂ in solution and vented directly to the gas chromatograph (GC, 9790II) for quantification of the gas products. The liquid

products of CO₂ reduction were identified and quantified by nuclear magnetic resonance (NMR, 500 MHz, Avance III).

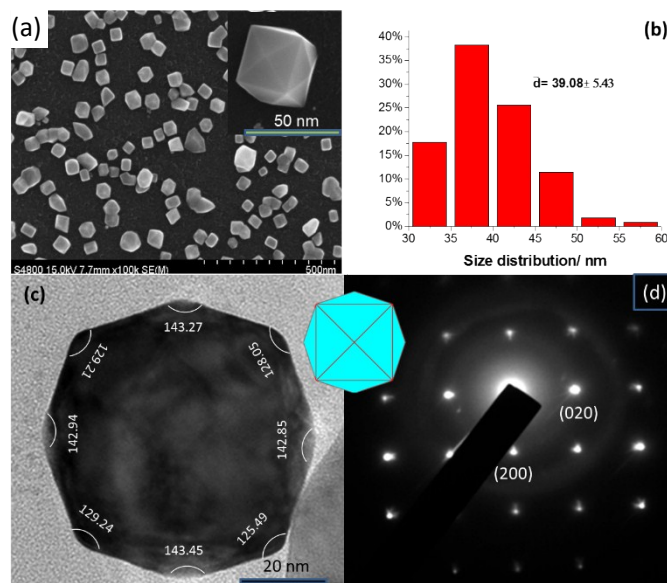


Fig. S1 (a) SEM images of THH Pd NCs, the inset show a magnified SEM image of a THH Pd NC; (b) the particle size histogram; (c) TEM image of a THH Pd NC along [001] zone axis, the surface facets were determined to be {310} by measuring the interfacial angles in the TEM image and comparing them with the theoretical values; (d) Corresponding SAED pattern of the THH Pd NC. The inset is a [001] projected model of a THH.

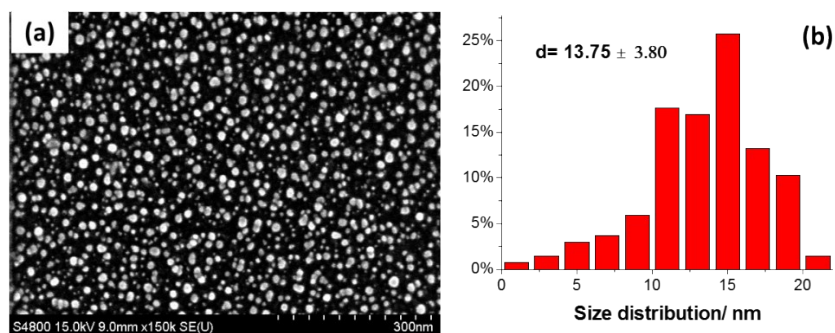


Fig. S2 (a) SEM images of the {111}-faceted Pd NCs; (b) the particle size histogram.

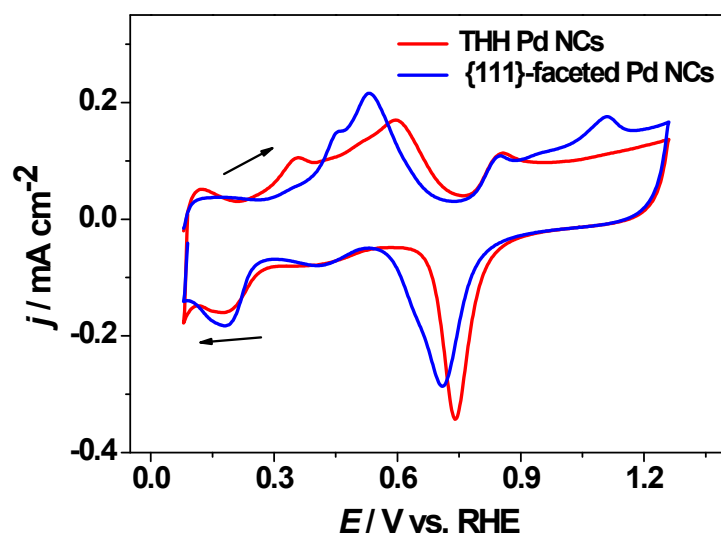


Fig. S3 Cu stripping on Cu modified THH Pd NCs and {111}-faceted Pd NCs in 0.5 M H_2SO_4 .

The Cu stripping on THH Pd NCs occurs at a more negative potential than that on (111)-faceted Pd NCs. It is clearly seen that the current of hydrogen region has been severely suppressed, and after Cu stripping, the hydrogen region recovered. The coverage of Cu is calculated according to the ratio between the charge of Cu stripping and that of hydrogen adsorption/desorption, considering a value of $420 \mu\text{C cm}^{-2}$ for Cu oxidation, and $210 \mu\text{C cm}^{-2}$ for hydrogen adsorption/desorption. The coverage of Cu is calculated to be 0.98 ML and 0.97 ML for THH Pd NCs and (111)-faceted Pd NCs, respectively. But for simplicity, they are denoted as $\text{Cu}_{1\text{ML}}/\text{THH Pd NCs}$ and $\text{Cu}_{1\text{ML}}/\{111\}$ -faceted Pd NCs, respectively.

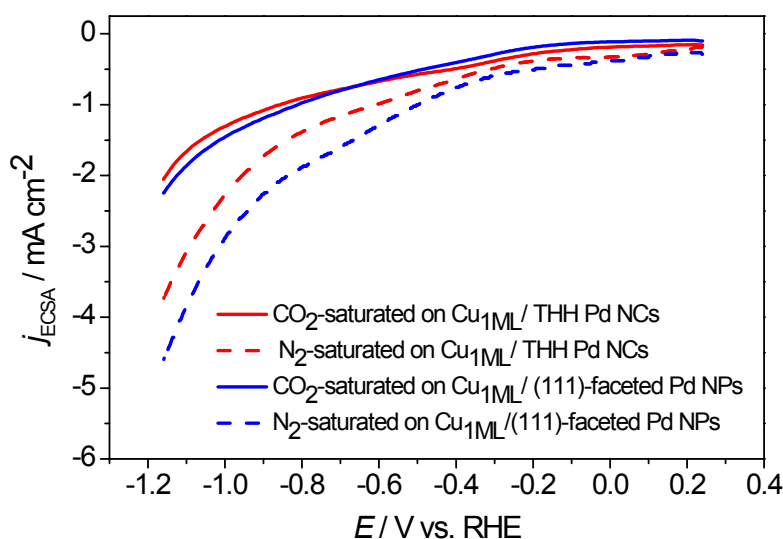


Fig. S4 Linear sweep voltammetry of electroreduction CO_2 on $\text{Cu}_{1\text{ML}}/\text{THH Pd NCs}$ (red line) and $\text{Cu}/\{111\}$ -faceted Pd NCs (blue line) in a CO_2 -saturated (solid line) and N_2 -saturated (dash line) in 0.1 M NaHCO_3 aqueous solution, respectively.

Linear sweep voltammetry was performed for the electroreduction of CO_2 . For both $\text{Cu}_{1\text{ML}}/\text{THH Pd NCs}$ and $\text{Cu}_{1\text{ML}}/\{111\}$ -faceted Pd NCs electrodes, the current densities in N_2 -saturated solution are higher than those in CO_2 -saturated solution, which might be caused

by the severely suppressed hydrogen evolution reaction (HER) in CO₂-saturated solution. This phenomenon is often seen in the literature on Pd electrodes.^{1,2}

Table S1 Faradaic efficiency (%) of products of CO₂ reduction on Cu_{1ML}/THH Pd NCs and Cu_{1ML}/(111)-faceted Pd NCs at different potentials.

E / V vs. RHE	Cu _{1ML} /THH Pd NCs					Cu _{1ML} /(111)-faceted Pd NCs				
	Ethanol	Methanol	CO	H ₂	total	Ethanol	Methanol	CO	H ₂	total
-0.36	11.9	0	7.0	77.2	96.1	5.7	4.9	10.0	70.1	90.7
-0.46	20.4	3.1	5.8	58.2	87.5	6.1	3.4	3.8	76.9	90.2
-0.56	12.5	5.7	1.7	74.4	94.3	8.0	6.7	1.8	81.1	97.6

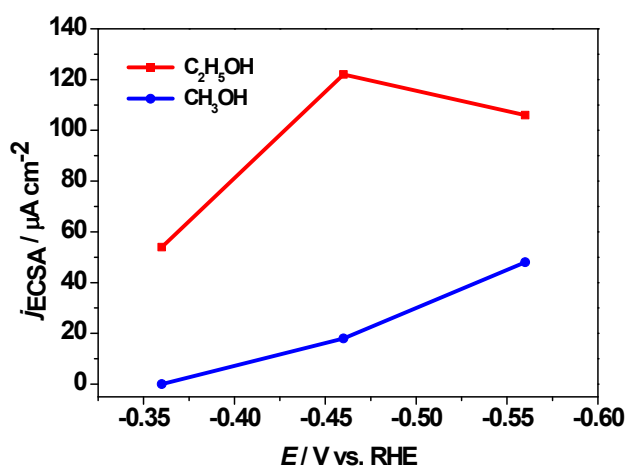


Fig. S5 Partial current density of methanol and ethanol from CO₂ electroreduction on Cu_{1ML}/THH Pd electrode at different potentials.

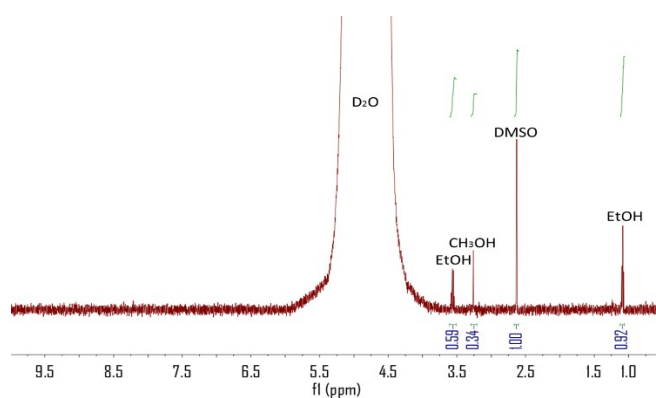


Fig. S6 NMR spectrum of the liquid products of CO₂ electroreduction on Cu_{1ML}/THH Pd NCs at -0.46 V vs. RHE.

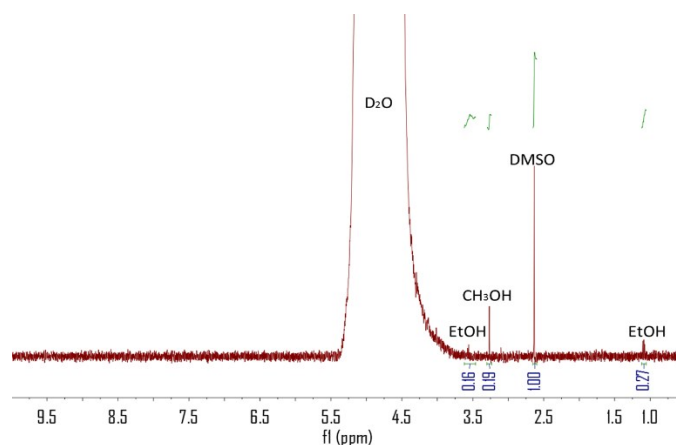


Fig. S7 NMR spectrum of the liquid products of CO₂ electroreduction on Cu_{1ML}/(111)-faceted Pd NCs at -0.46 V vs. RHE.

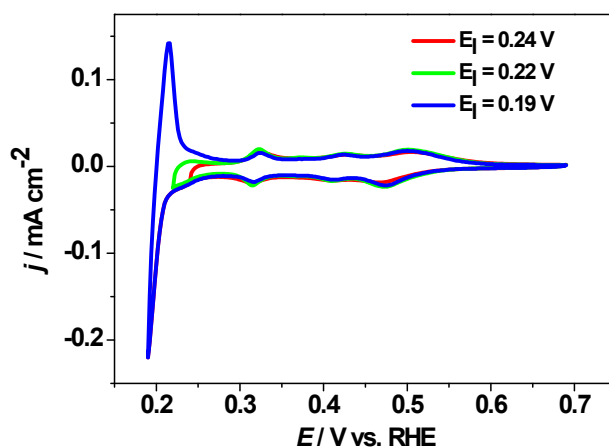


Fig. S8 Cu electrodeposition on THH Pd NCs, by cyclic voltammetry with different low potential limits at 0.24, 0.22, and 0.19 V, respectively. Solution: 1 mM CuSO₄ + 0.5 M H₂SO₄, scan rate: 10 mVs⁻¹.

Fig. S8 shows the Cu electrodeposition on THH Pd NCs by cyclic voltammetry with different low potential limits at 0.24, 0.22, and 0.19 V, respectively, and the final potential was set at the low potential limit, in 1 mM CuSO₄ + 0.5 M H₂SO₄. The lower the low potential limit is, the more amount of Cu can be electrodeposited.

Table S2 Faradaic efficiency (%) of products of CO₂ reduction on Cu modified THH Pd NCs with different Cu coverage by cyclic voltammetry of different low potential limits of 0.24, 0.22, and 0.19 V.

	Faradaic efficiency (%)				
	CH ₃ OH	C ₂ H ₅ OH	CO	H ₂	total
Cu _{0.8ML} /THH Pd NCs	19.5	5.8	16.9	62.3	104.5
Cu _{1ML} /THH Pd NCs	3.1	20.4	5.8	58.2	87.5
Cu _{1.2ML} /THH Pd NCs	3.0	5.3	5.9	70.6	84.8

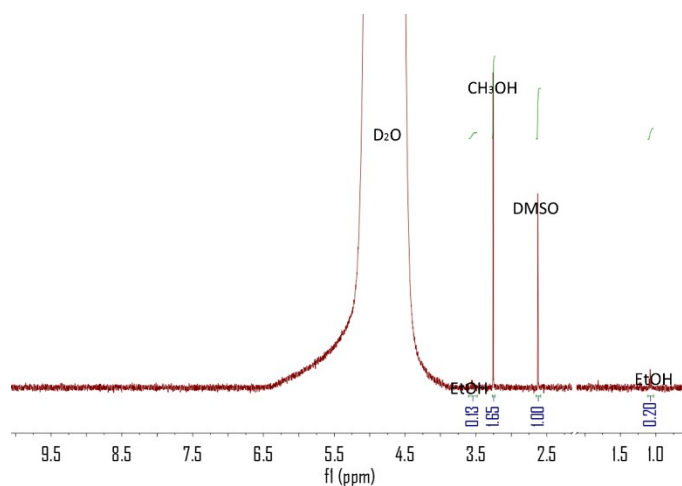


Fig. S9 NMR spectrum of the liquid products of CO₂ electroreduction on Cu_{0.8ML}/THH Pd NCs at -0.46 V vs. RHE.

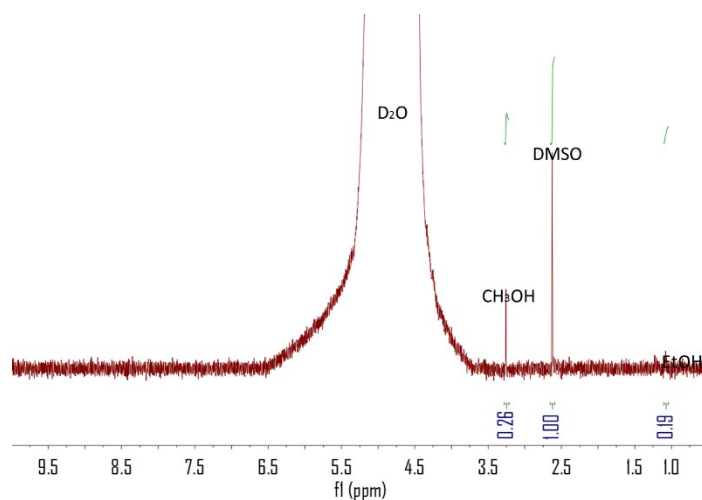


Fig. S10 NMR spectrum of the liquid products of CO₂ electroreduction on Cu_{1.2ML}/THH Pd NCs at -0.46 V vs. RHE.

Table S3 Comparison of performance of Cu_{1ML}/THH Pd NCs and Cu_{0.8ML}/THH Pd NCs catalysts with the reported catalysts for the electroreduction of CO₂ to ethanol and methanol

Catalyst	<i>E</i> / V vs. RHE	Electrolyte (pH)	Ethanol	Methanol	Reference
Cu _{1ML} /THH Pd NCs	-0.46	0.1 M NaHCO ₃ (6.8)	20.4%	3.1%	This study
Cu _{0.8ML} /THH Pd NCs	-0.46	0.1 M NaHCO ₃ (6.8)	5.8%	19.5%	This study

Cu ₂ O-based GDEs	-0.75	0.5 M KHCO ₃ (7.2)	10.1%	42.3%	3
Cu ₂ O/ZnO-based GDEs	-0.52	0.5 M KHCO ₃ (7.2)	3.5%	27.25%	3
Cu ₄ Zn	-1.05	0.1 M KHCO ₃ (6.8)	29.1%	NR	4
polycrystalline Cu	-1.05	0.1 M KHCO ₃ (6.8)	9.75%	0.02%	5
Cu(100)	-1.0	0.1 M KHCO ₃ (6.8)	6.49%	NR	6
Cu(111)	-1.1	0.1 M KHCO ₃ (6.8)	4.08%	NR	6
Cu(110)	-1.05	0.1 M KHCO ₃ (6.8)	7.41%	NR	6
10 nm CuO nanoparticles	-1.13	CO ₂ -saturated 0.2 M KI (5.6)	34.1%	trace	7
7.3 μm Cu nanowire	-1.1	0.1 M KHCO ₃ (6.8)	5.0%	NR	8
NGQDs	-0.78	1 M KOH (14)	16%	NR	7
Cu/CNS	-1.2	0.1 M KHCO ₃ (6.8)	63%	NR	10
Cu	-1.0	0.1 M CsHCO ₃ (6.8)	11.4%	NR	11
Cu _{63.9} Au _{36.1}	-0.43	0.5 M KHCO ₃ (7.3)	12%	15.9%	12
HKUST-1	-0.23	0.5 M KHCO ₃ (7.3)	10.3%	5.6%	13
CuDAT-wire	-0.50	1 M KHCO ₃ (13.5)	20%	NR	14
[PYD]@Pd	-0.03	CO ₂ -saturated 0.5 M KCl (5.6)	NR	35%	15
3.6 μm Cu ₂ O film	-0.99	0.1 M KHCO ₃ (6.8)	16.37	NR	16
Cu ₂ O-derived Cu	-1.0	0.1 M KHCO ₃ (6.8)	16.4%	NR	17

Abbreviations: GDEs, gas diffusion electrodes; NGQDs, N-doped graphene quantum dots; CNS, N-doped carbon nanospire; HKUST-1, [Cu₃(μ₆-C₉H₃O₆)₂]; DAT, 3,5-diamino-1,2,4-triazole; NR, not reported.

Computational methods

The electronic structure calculations were performed using the Vienna Ab-initio Simulation Package (VASP) code with the exchange-correlation functional of Perdew-Burke-Ernzerhof (PBE). The projector-augmented-wave (PAW) pseudopotentials were utilized to describe the core electron interaction.¹⁸⁻²² The Pd(310) surface was modeled by a *p*(3x1) unit cell including 48 Pd atoms, and a 2x3x1 Monkhorst-Pack *k*-point sampling was used. Cu atoms were gradually added on the Pd(310) surface until to 1.67 ML, as shown in **Fig. S11**. The vacuum region was ~12 Å to ensure that there is a little interaction between slabs. One CO molecule adsorbs on the step top site and terrace bridge site, respectively for calculating the adsorption energy. The free energy was defined as: $G_{ad} = G_{CO/slab} - G_{CO} - G_{slab}$, in which $G_{CO/slab}$, G_{CO} , and G_{slab} are the total energies of the adsorbate binding with surface, gaseous adsorbate and clean surface, respectively.

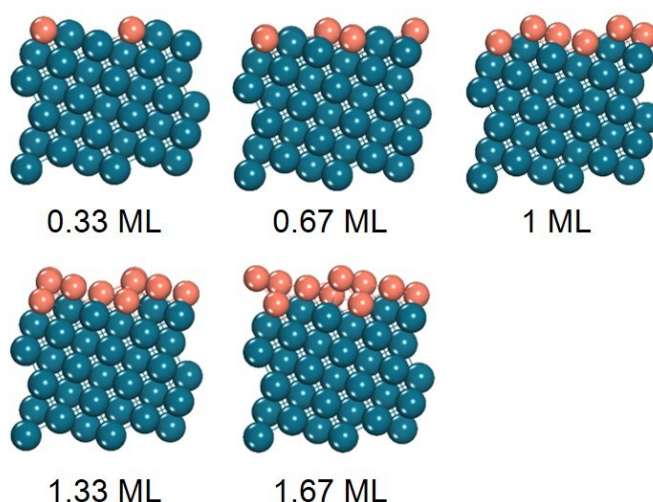


Fig. S11 Side views of the model of Cu modified Pd(310) surface. The Cu coverage is increased from 0.33 ML to 1.67 ML. Orange: Cu; blue: Pd.

References

1. D. Gao, H. Zhou and X. Bao, *Nano Research*, 2017, **10**, 2181-2191.
2. R. Kortlever, C. Balemans, Y. Kwon and M. T. M. Koper, *Catal. Today*, 2015, **244**, 58-62.
3. J. Albo and A. Irabien, *J. Catal.*, 2015, **343**, 232-239.
4. D. Ren, B. S.-H. Ang and B. S. Yeo, *ACS Catal.*, 2016, **6**, 8239-8247.
5. K. P. Kuhl, E. R. Cave, D. N. Abram and T. F. Jaramillo, *Energy & Environ. Sci.*, 2012, **5**, 7050.
6. Y. Huang, A. D. Handoko, P. Hirunsit and B. S. Yeo, *ACS Catalysis*, 2017, **7**, 1749-1756.
7. D. Chi, H. Yang, Y. Du, T. Lv, G. Sui, H. Wang and J. Lu, *RSC Adv.*, 2014, **4**, 37329.
8. M. Ma, K. Djanashvili and W. A. Smith, *Angew. Chem. Int. Ed.*, 2016, **55**, 6680-6684.
9. J. Wu, S. Ma, J. Sun, J. I. Gold, C. Tiwary, B. Kim, L. Zhu, N. Chopra, I. N. Odeh, R. Vajtai, A. Z. Yu, R. Luo, J. Lou, G. Ding, P. J. Kenis and P. M. Ajayan, *Nat. Commun.*, 2016, **7**, 13869.
10. Y. Song, R. Peng, D. K. Hensley, P. V. Bonnesen, L. Liang, Z. Wu, H. M. Meyer, M. Chi, C. Ma, B. G. Sumpter and A. J. Rondinone, *ChemistrySelect*, 2016, **1**, 6055-6061.
11. M. R. Singh, Y. Kwon, Y. Lum, J. W. Ager, 3rd and A. T. Bell, *J. Am. Chem. Soc.*, 2016, **138**, 13006-13012.
12. F. Jia, X. Yu and L. Zhang, *J. Power Sources*, 2014, **252**, 85-89.
13. a. Jonathan Albo and a. A. Irabien, *ChemSusChem*, 2017, **10**, 1100-1109.
14. T. T. H. Hoang, S. Ma, J. I. Gold, P. J. A. Kenis and A. A. Gewirth, *ACS Catal.*, 2017, **7**, 3313-3321.
15. H.-P. Yang, S. Qin, H. Wang and J.-X. Lu, *Green Chem.*, 2015, **17**, 5144-5148.
16. D. Ren, Y. Deng, A. D. Handoko, C. S. Chen, S. Malkhandi and B. S. Yeo, *ACS Catalysis*, 2015, **5**, 2814-2821.
17. C. S. Chen, J. H. Wan and B. S. Yeo, *J. Phys. Chem. C*, 2015, **119**, 26875-26882.
18. G. Kresse, J. Hafner, *Phys. Rev. B*, 1993, **48**, 13115.
19. G. Kresse, J. Furthmuler, *Phys. Rev. B*, 1996, **54**, 11169.
20. P. E. Blochl, *Phys. Rev. B*, 1994, **50**, 17953.
21. J. P. Pedrew, K. Burke, *Phys. Rev. Lett.*, 1996, **77**, 3865.
22. J. P. Pedrew, K. Burke, M. Ernzerhof, *Phys. Rev. Lett.*, 1997, **78**, 1396.